Accuracy of sun localization in the second step of sky-polarimetric Viking navigation for north determination: a planetarium experiment

Alexandra Farkas,[1,5] Dénes Száz,[1,6] Ádám Egri,[1,2,7] Miklós Blahó,[1,8] András Barta,[1,2,9] Dóra Nehéz,[3,10] Balázs Bernáth,[1,4,11] and Gábor Horváth[1,*]

[1]*Environmental Optics Laboratory, Department of Biological Physics, Physical Institute, Eötvös University, H-1117 Budapest, Pázmány sétány 1, Hungary*
[2]*Estrato Research and Development Ltd., H-1121 Budapest, Mártonlak utca 13, Hungary*
[3]*Department of Astronomy, Institute of Geography and Earth Sciences, Eötvös University, H-1117 Budapest, Pázmány sétány 1, Hungary*
[4]*Institute of Biology, University of Neuchatel, Rue Emile-Argand 11, CH-2000 Neuchatel, Switzerland*
[5]*e-mail: kfarkasalexandra@gmail.com*
[6]*e-mail: szaz.denes@gmail.com*
[7]*e-mail: adamp39@gmail.com*
[8]*e-mail: majkl2000@gmail.com*
[9]*e-mail: bartaandras@gmail.com*
[10]*e-mail: nehez.dori@gmail.com*
[11]*e-mail: bbernath@angel.elte.hu*
**Corresponding author: gh@arago.elte.hu*

Received April 17, 2014; accepted May 13, 2014;
posted May 23, 2014 (Doc. ID 210274); published June 30, 2014

It is a widely discussed hypothesis that Viking seafarers might have been able to locate the position of the occluded sun by means of dichroic or birefringent crystals, the mysterious sunstones, with which they could analyze skylight polarization. Although the atmospheric optical prerequisites and certain aspects of the efficiency of this sky-polarimetric Viking navigation have been investigated, the accuracy of the main steps of this method has not been quantitatively examined. To fill in this gap, we present here the results of a planetarium experiment in which we measured the azimuth and elevation errors of localization of the invisible sun. In the planetarium sun localization was performed in two selected celestial points on the basis of the alignments of two small sections of two celestial great circles passing through the sun. In the second step of sky-polarimetric Viking navigation the navigator needed to determine the intersection of two such celestial circles. We found that the position of the sun (solar elevation θ_S, solar azimuth φ_S) was estimated with an average error of $+0.6° \leq \Delta\theta \leq +8.8°$ and $-3.9° \leq \Delta\varphi \leq +2.0°$. We also calculated the compass direction error when the estimated sun position is used for orienting with a Viking sun-compass. The northern direction (ω_{North}) was determined with an error of $-3.34° \leq \Delta\omega_{\mathrm{North}} \leq +6.29°$. The inaccuracy of the second step of this navigation method was high ($\Delta\omega_{\mathrm{North}} = -16.3°$) when the solar elevation was $5° \leq \theta_S \leq 25°$, and the two selected celestial points were far from the sun (at angular distances $95° \leq \gamma_1, \gamma_2 \leq 115°$) and each other ($125° \leq \delta \leq 145°$). Considering only this second step, the sky-polarimetric navigation could be more accurate in the mid-summer period (June and July), when in the daytime the sun is high above the horizon for long periods. In the spring (and autumn) equinoctial period, alternative methods (using a twilight board, for example) might be more appropriate. Since Viking navigators surely also committed further errors in the first and third steps, the orientation errors presented here underestimate the net error of the whole sky-polarimetric navigation.

OCIS codes: (000.4930) Other topics of general interest; (010.1290) Atmospheric optics; (260.1180) Crystal optics; (260.5430) Polarization; (330.5510) Psychophysics; (330.7321) Vision coupled optical systems.
http://dx.doi.org/10.1364/JOSAA.31.001645

1. INTRODUCTION

A millennium ago, the Vikings (Norse people from Scandinavia) routinely sailed on the high seas, traded with civilizations of the Middle East, plundered the West European coasts, settled down in Greenland, and explored and discovered the coasts of North America [1]. Many details were revealed about their ship-building technology from well-conserved shipwrecks [2], but their navigational discipline is still mysterious. Based on an 11th century artifact found at Uunartoq in Greenland, the scientific community accepted that they might have navigated on the open sea under sunny meteorological conditions with sun-compasses. These instruments bear gnomonic lines valid at a given latitude on prominent dates (e.g., spring equinox, summer solstice) and provide compass directions with the aid of the gnomon shadow [3]. Recently, two alternative interpretations of the Uunartoq artifact were demonstrated: it was interpreted as an instrument to determine latitude and local noon [4], or as a twilight board [5]. It is a frequently cited and often criticized hypothesis that Vikings were able to locate the sun and perform solar navigation even under cloudy or foggy conditions with a three-step sky-polarimetric navigation [6]:

Step 1 (Fig. 1A): Viking navigators are assumed to have determined the direction of skylight polarization in at least two celestial points with the use of two sunstones to estimate the position of the sun occluded by cloud/fog or being below the horizon. The alleged tools for this task are the mysterious sunstones, the composition and usage of which are unknown, but their high value is sure [7]. It has been hypothesized that sunstones were birefringent (e.g., calcite) or dichroic (e.g., cordierite or tourmaline) crystals. A recent archaeological artifact raised the possibility that calcite crystals were used for navigation purposes even in the 16th century [8].

Step 2 (Fig. 1B): A short scratch on each sunstone could help the navigator to set two celestial great circles across the two investigated sky points parallel to the scratches being perpendicular to the local direction of skylight polarization. Then the navigator determined the above-horizon intersection of these celestial circles. According to the Rayleigh theory of sky polarization [9], this intersection coincides with the position of the invisible sun.

Step 3 (Fig. 1C): Finally, from the estimated position of the invisible sun the navigator derived true compass directions. Since no astronomical charts are known from the Viking area before the 12th century, the method of the third step can only be speculated. Probably, it involved the use of a sun-compass, the fragment of which was found at Uunartoq, for example. The navigator might have determined the direction of the imaginary light rays originating from the invisible sun with a shadow-stick [10]. Then, he turned the horizontal disk of the sun-compass around its vertical axis of rotation, until the tip of the imaginary shadow of the vertical compass gnomon reached the actual gnomonic line engraved into the disk [5]. In this situation the mirror symmetry axis of the gnomonic line pointed toward the geographical north.

The atmospheric optical prerequisites and the overall efficiency of this sky-polarimetric Viking navigation have been intensively investigated, and its plausibility was questioned or supported by several researchers [11–18]. Although the

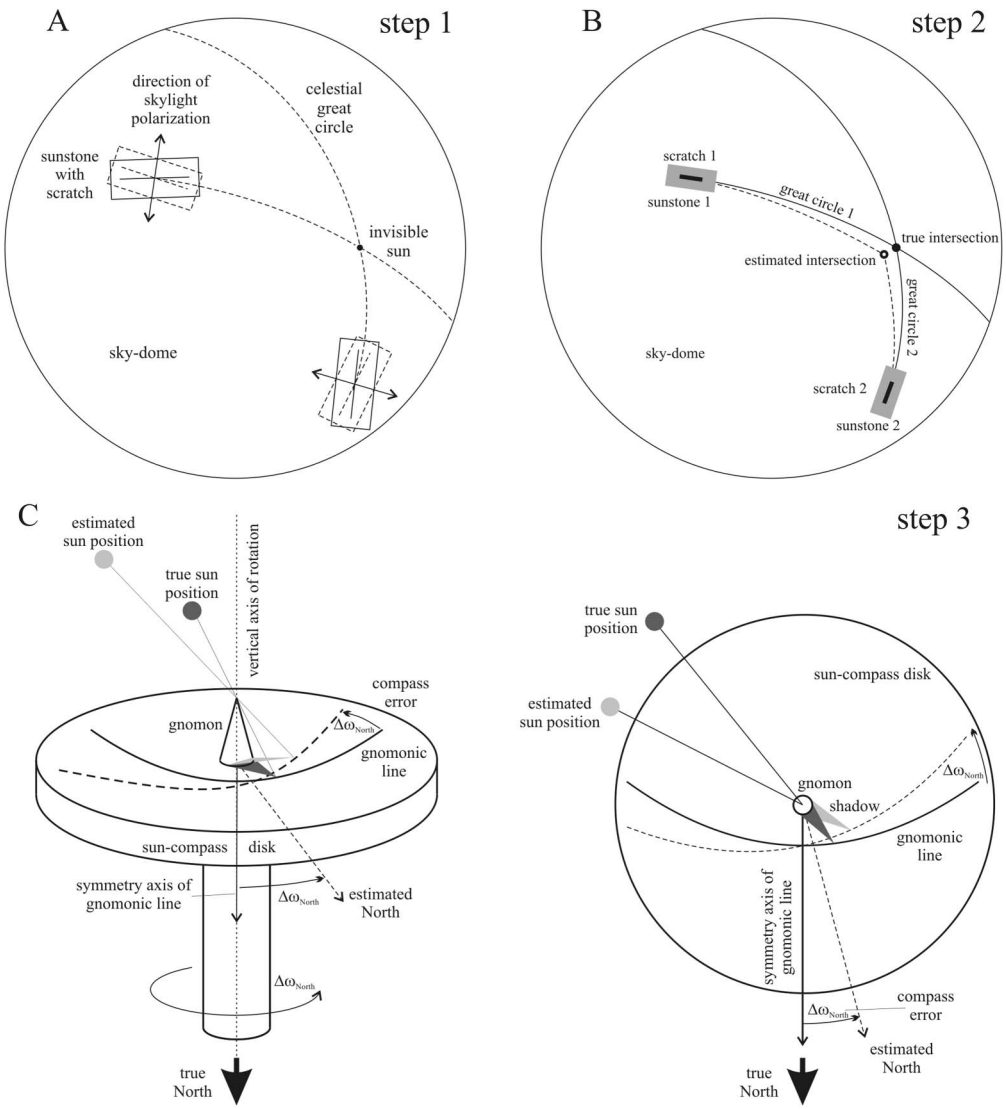

Fig. 1. Three main steps of sky-polarimetric Viking navigation. A, step 1: estimation of the direction of skylight polarization with sunstones. B, step 2: estimation of the intersection of the two celestial great circles across the selected two sky points and parallel to the scratches on the sunstones. C, step 3: estimation of the northern direction with the Viking sun-compass (left, side view of the sun-compass; right, sun-compass disk seen from above). Further details in the text.

accuracy of sky polarimetry with sunstones and various methods of deriving true directions from the sun position have been studied before [5,10,16], accurate estimation of the sun position with such a sky-polarimetric method had been taken for granted. However, this is not a simple task, even for experienced observers. The human mind is accustomed to perspective and extending straight lines that meet in vanishing points along the horizon, but not to elongating short sections of great circles in the celestial hemisphere as step 2 of Viking navigation requires. This inadequate routine may greatly influence the observers, especially if they have the task of appointing celestial points near the horizon, where visual objects appear in their everyday life. The accuracy of estimating the sun position (intersection of the two celestial great circles) may depend strongly on the solar elevation angle. The error of estimation is expected to increase, if the angle between the planes of the mentioned two circles progressively deviates from 90°, or the two small sections of these circles are far from their intersection.

We present here the results of a planetarium experiment that investigated the earlier unknown accuracy of the second step of sky-polarimetric Viking navigation (Fig. 1B). We measured the error of localization of the invisible sun, when the navigator already knows the direction of the celestial great circles passing through the sun in two sky points, and his task is to determine the intersection of these two circles coinciding with the invisible sun. From the measured sun localization errors of the second step (Fig. 1B) we derived the accuracies of determining the compass direction (north) by means of a Viking sun-compass with the assumption that the errors of the first (Fig. 1A) and third (Fig. 1C) navigational steps were zero. The results of our study are essential to establish the accuracy of the alleged sky-polarimetric Viking navigation and to judge the plausibility of this hypothesis.

2. MATERIALS AND METHODS

A. Planetarium Experiment

The test persons of our experiment were 11 city-dwelling male volunteers aged between 23 and 63 years. The experiment was performed in the digital planetarium of Eötvös University in Budapest (Hungary) in 2013. This planetarium has a dome diameter of 8 m and uses a fixed central single-lens Digitarium ε projector (Digitalis Education Solutions, Inc., Bremerton, USA) provided with Nightshade 11.12.1 software and a circumferential resolution of 2400 pixels.

The test persons sat in the immediate vicinity (30 cm) of the planetarium projector with their eye level about 5 cm below the projector lens in order to minimize parallax error and to avoid being dazzled by the projector. Two thin (0.6°) black bars with an angular length of 5° were projected in two different points of the white planetarium dome (Figs. 2 and 3). Since the white dome canvas was composed of several sectors, a pale radial pattern with a perpendicular circle formed by the sector junction lines was visible on it. The task of the test persons was (i) to elongate imaginarily (mentally) each bar to a spherical great circle, (ii) to locate the intersection of these two circles, and (iii) to mark the intersection with a green laser pointer on the planetarium dome, which represented the sky dome. The intersection represented the position of the invisible sun, while the black bars modeled the

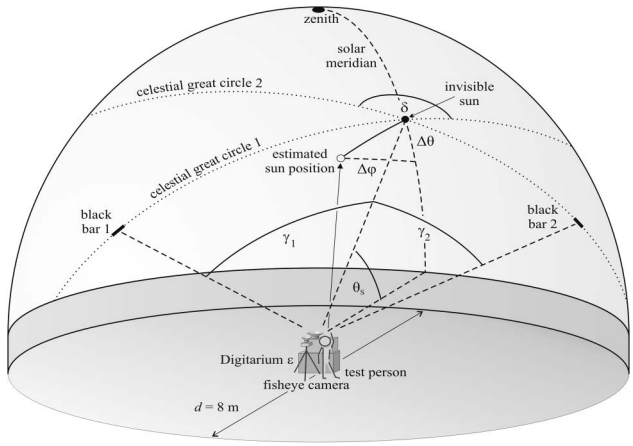

Fig. 2. Geometry of our planetarium experiment with the Digitarium ε projector in the center, the test person, the fisheye camera, and the two black bars projected onto the white planetarium dome with a diameter $d = 8$ m. The sun position to be guessed by the test person is at the above-horizon intersection of the two celestial great circles 1 and 2 passing through and parallel to the black bars 1 and 2. There are four free parameters: solar elevation angle θ_S, angular distances γ_1 and γ_2 of the center of bars 1 and 2 from the sun, and angle δ between the planes of circles 1 and 2. The test person marked the estimated sun position with a green laser spot. $\Delta\varphi$ and $\Delta\theta$ are the azimuth error and the elevation error, respectively, between the real and estimated sun positions. The bottom of the dome was at $\theta_{\text{dome}} = 8°$ above the real horizon being at the eye level of the test person.

hypothesized short scratches engraved in Viking sunstones and pointing toward the sun along celestial great circles [8,10,18]. The horizontal circular bottom edge of the planetarium dome was by $\theta_{\text{dome}} = 8°$ above the eye level of the test persons. Thus, the images were projected onto the dome with an appropriate slight zoom. Although the test persons had the possibility to point the green laser spot on the vertical cylindrical wall under the dome bottom, green spots projected below eye level were not accepted; i.e., we tested only situations in which the sun was above the horizon. After estimating the intersection of the two great circles (i.e., the sun position), the test persons did not see the correct solution (the correct position of the invisible sun). Thus, they were not influenced by any information feedback.

Besides the two black bars, a red, a blue, and a violet calibration spot were also projected on the planetarium dome (Fig. 3). They were used later as beacons in the evaluation process. These colored spots were projected at elevation $\theta = 10°$ with $\varphi = 120°$ azimuth angle difference between the neighboring spots. The calibration spots could not provide assistance for the test persons, because they were projected onto the dome with a random azimuth rotation.

We classified the measurement situations according to the following four free parameters (Fig. 2): (1) solar elevation angle θ_S, (2), (3) angular distance γ_1 and γ_2 of the center of bar 1 and bar 2 from the sun (intersection of the two great circles going across and parallel to the two bars), and (4) angle δ between the planes of the two great circles. The values of these four parameters were divided into ranges of 30°. The parameter values were chosen from the middle 20° interval of each range to make the ranges more separable from each other. Only realistic range combinations were used, which could really occur at the geographical areas where Vikings lived (Table 1). We generated situations for the solar elevation

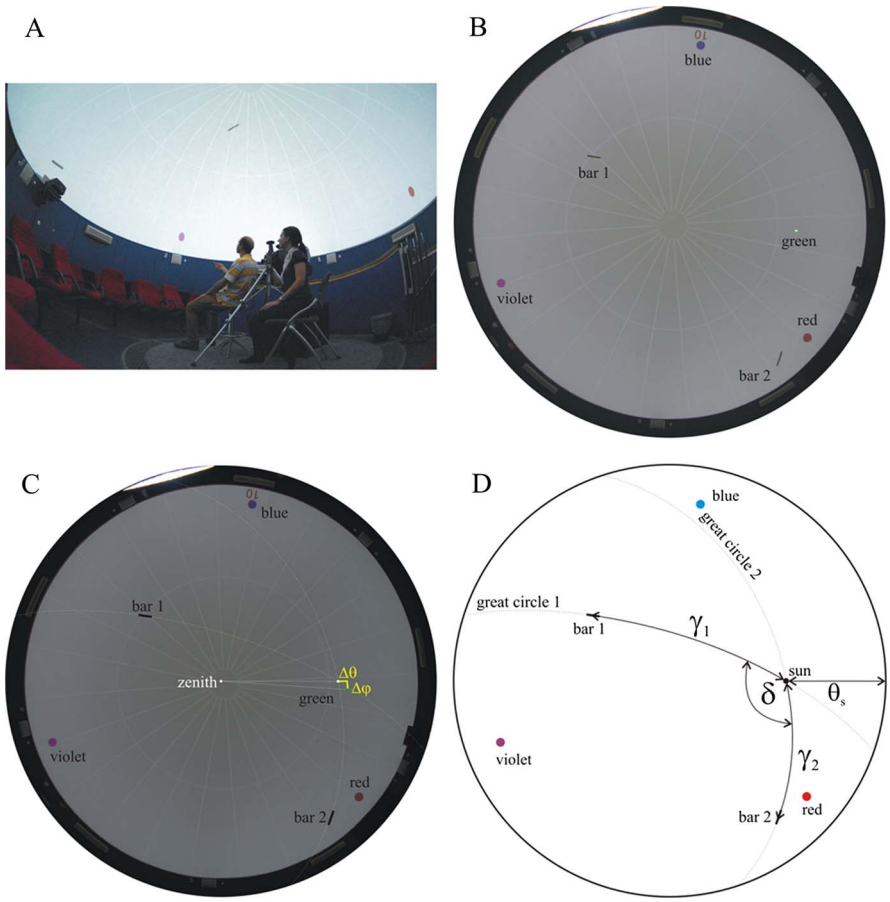

Fig. 3. A, the test person sat immediately next to the planetarium projector almost at the center of the hemispherical dome. He was instructed by the experiment leader (i) to observe the two black bars projected onto the white dome, (ii) to estimate the position of the invisible sun (i.e., the intersection of the two great circles passing through and parallel to the bars), and (iii) to mark the position of the estimated intersection with a green laser spot. The instructor of the experiment photographed the dome by a fisheye camera with a vertical optical axis. The pale radial pattern (composed of a circular and 24 radial thin white lines) visible on the white dome originated from the structure of the canvas composed of several sectors. B, example for the image projected onto the planetarium dome showing a measurement situation with the two black bars, and the three (red, blue, violet) calibration spots at an elevation $\theta = 10°$. The number under the blue spot codes the image number of the script file. In this example, the values of the four free parameters of the black bars were $\theta_S = 41°$, $\gamma_1 = 84°$, $\gamma_2 = 50°$, and $\delta = 129°$. C, the azimuth error $\Delta\varphi$ and the elevation error $\Delta\theta$ between the real sun position (white dot) and the estimated sun position (green dot) were calculated after the undistortion and appropriate rotation of the photographed calibration image (PCI). D, the sun is positioned at the intersection ($\varphi_S = 0$, $\theta = \theta_S$). The arcs of the two great circles across and parallel to black bars 1 and 2 were not projected during the tests.

angle θ_S from 5°–25° to 35°–55°, because $\theta_S > 55°$ does not occur along the 61° northern latitude, where Vikings regularly sailed between Scandinavia and Greenland (the highest possible solar elevation angle at the 61° northern latitude is $\theta_S = 52.5°$, if refraction is neglected). Because of the Arago, Babinet, and Brewster neutral (unpolarized) points of the sky [9,19–21], the measurement of skylight polarization with sunstones is impossible at and around the sun and antisolar point. Therefore, we omitted situations with $\gamma_1, \gamma_2 < 30°$ and $\gamma_1, \gamma_2 > 150°$. We also avoided situations with $120° < \gamma_1, \gamma_2 < 150°$, because in the case of higher solar elevations the projected black bars would have been positioned below the horizon. By generating random settings of the four free parameters ($\theta_S, \gamma_1, \gamma_2, \delta$) within the ranges defined in Table 1, we obtained 48 parameter configurations. Using our custom-made computer program, 240 individual situations were created in stereographic bitmap images with 2048×2048 pixel resolution by generating five images for all 48 configurations. A circle with a radius of 1024 pixels represented the horizon, and the center of this circle corresponded to the zenith in the planetarium dome. The azimuth angle φ and the elevation angle θ of an arbitrary point with a position vector p on the dome were defined in the following way:

Table 1. Ranges of the Solar Elevation Angle θ_S, the Angular Distances γ_1 and γ_2 between the Sun and Two Selected Celestial Points, and the Angle δ Enclosed by the Planes of the Two Celestial Great Circles Passing through the Two Celestial Points Parallel to Two Black Bars Projected onto the White Planetarium Dome in Our Experiment[a]

θ_S	γ_1	γ_2	δ
5°–25°	35°–55°	35°–55°	35°–55°
35°–55°	65°–85°	65°–85°	65°–85°
—	95°–115°	95°–115°	95°–115°
—	—	—	125°–145°

[a]Combinations of these angle ranges defined the 48 situations in which the test persons had to estimate the position of the invisible sun, i.e., the intersection of the two celestial great circles across the two black bars.

$$\varphi = \begin{cases} \arctan\left(\frac{(\underline{o}-\underline{p})_y}{(\underline{o}-\underline{p})_x}\right), & \text{if} \quad (\underline{o}-\underline{p})_x > 0 \\ \arctan\left(\frac{(\underline{o}-\underline{p})_y}{(\underline{o}-\underline{p})_x}\right) + \pi, & \text{if} \quad (\underline{o}-\underline{p})_y \geq 0, (\underline{o}-\underline{p})_x < 0 \\ \arctan\left(\frac{(\underline{o}-\underline{p})_y}{(\underline{o}-\underline{p})_x}\right) - \pi, & \text{if} \quad (\underline{o}-\underline{p})_y < 0, (\underline{o}-\underline{p})_x < 0 \\ +\frac{\pi}{2}, & \text{if} \quad (\underline{o}-\underline{p})_y > 0, (\underline{o}-\underline{p})_x = 0 \\ -\frac{\text{phiv}}{2}, & \text{if} \quad (\underline{o}-\underline{p})_y < 0, (\underline{o}-\underline{p})_x = 0 \\ \text{undefined}, & \text{if} \quad (\underline{o}-\underline{p})_y = 0, (\underline{o}-\underline{p})_x = 0 \end{cases}, \tag{1}$$

$$\theta = 90° - \frac{|\underline{o}-\underline{p}|}{r} \cdot 90°, \tag{2}$$

where $\underline{o}$ is the position vector of the image center, and r is the image radius. During the image generation process we first defined the position of the sun with a given solar elevation angle θ_S. The images were projected onto the planetarium dome with a randomized azimuth rotation; therefore we defined the azimuth angle of the sun as $\varphi_S = 0$. Then, two celestial great circles with an angle δ between their planes were considered, which intersected each other at the sun position to be guessed by the test persons (Figs. 1B, 2, and 3D). The positions of the black bars were calculated on the basis of their chosen angular distances γ_1 and γ_2 from the sun. Finally, the 5° segments of the two great circles were drawn at the centers of the two bars.

The generated images were projected onto the planetarium dome using the StratoScript 2.2 scripting language. We presented the same 240 situations to all 11 test persons in a randomized order and with a random azimuth rotation. This resulted in 2640 individual estimations of the position of the invisible sun. All test persons were provided with a total of six series of 40 situations, and were allowed to survey a maximum of two series on a single day with 20 min of intermission.

B. Data Registration and Evaluation

The white reflective planetarium dome with the two black bars, the three colored calibration spots, and the green laser spot positioned by a given test person was photographed with a Nikon Coolpix 8700 digital camera having a Nikon FC-E8 fisheye converter lens with a vertical optical axis. This camera was fixed on a tripod placed right next to the projector. Since the projector was positioned at the planetarium center, the camera had to be placed slightly off the dome center and perceived a slightly distorted version of the projected image. To compensate this, the fisheye photographs were transformed. A calibration image (CI) consisting of a grid of 20 concentric and 16 radial calibration lines was projected onto the dome (Fig. 4) and photographed at the beginning of each

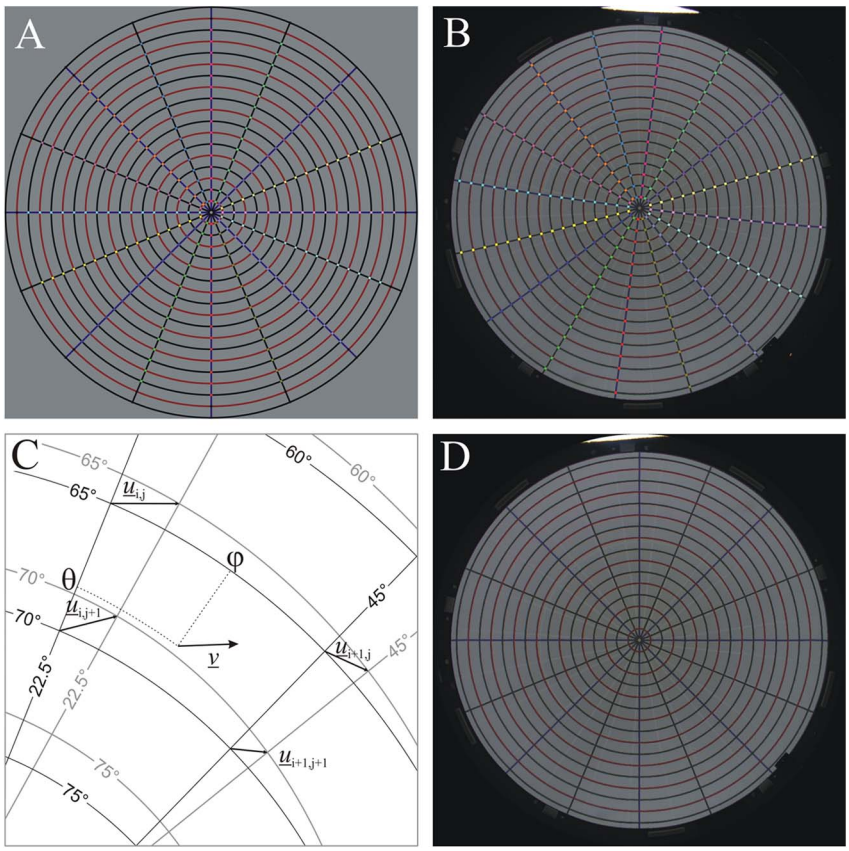

Fig. 4. Undistortion procedure of the 180° field-of-view photographs taken about the planetarium dome. A, Calibration image (CI) projected before each script with specific colored spots placed on the grid points. B, slightly off-axis and off-center photograph of the dome with the photographed calibration image (PCI). Recognition of the appropriate grid point pairs was performed with the help of the colored spots that mark the grid points. C, the black and gray nets represent the grid in the CI and PCI, respectively. The recognized vectors of the grid points were used to calculate the correct pixel colors for each pixel: the $\underline{v}$ vector is interpolated from the bracketing $\underline{u}_{i,j}$, $\underline{u}_{i+1,j}$, $\underline{u}_{i,j+1}$, and $\underline{u}_{i+1,j+1}$ vectors. D, result of the undistortion procedure performed on the PCI.

experiment session. This photographed calibration image (PCI) was used in the further evaluation.

Spots with a diameter of 9 pixels and specific colors were manually placed on the grid points of both CI and PCI. A self-developed software recognized these spots and calculated the coordinates of their centers. A so-called undistortion vector $\underline{v}$ was calculated between the spots on the CI and their counterparts on the PCI for each pair by subtracting all of the spots' center positions on the PCI from those of the counterparts on the CI. This produced an $\boldsymbol{u}_{\underline{i},j}$ ($i = 0, \ldots, 16$ azimuth index; $j = 0, \ldots, 18$ elevation index) array with $\Delta_\varphi = 22.5°$ and $\Delta_\theta = 5°$ azimuth and elevation resolution, respectively. For arbitrary (φ, θ) pairs the undistortion vector $\underline{v}$ was calculated with linear interpolation:

$$\begin{aligned} \underline{v} &= (1-\tilde{\varphi})\cdot(1-\tilde{\theta})\cdot \underline{u}_{i,j} + (1-\tilde{\varphi})\cdot\tilde{\theta}\cdot\underline{u}_{i,j+1} \\ &\quad + \tilde{\varphi}\cdot(1-\tilde{\theta})\cdot\underline{u}_{i+1,j} + \tilde{\varphi}\cdot\tilde{\theta}\cdot\underline{u}_{i+1,j+1}, \\ \tilde{\varphi} &= \frac{\phi - i\cdot\Delta_\varphi}{\Delta_\varphi}, \qquad \tilde{\theta} = \frac{\theta - j\cdot\Delta_\theta}{\Delta_\theta}, \end{aligned} \tag{3}$$

where $\underline{u}_{i,j}$, $\underline{u}_{i+1,j}$, $\underline{u}_{i,j+1}$, and $\underline{u}_{i+1,j+1}$ are the four vectors in the calibration array (Fig. 4C). Hence, we defined a map for the undistortion as a bilinear interpolation of translation vectors obtained in the nodes of the radial calibration pattern. Note that there are more accurate methods to perform such a calibration (e.g., through determining radial distortion of both the projector and camera and calculating a projection matrix that translates between the undistorted, projected sky hemisphere to the slightly decentered view seen by the camera), but the accuracy of our method is good enough compared to the average measure of inaccuracies regarding the inferred sun position and northern direction.

After obtaining the $\boldsymbol{u}_{\underline{i},j}$ array, the same was performed for all fisheye photographs taken during a given experimental session in order to construct the undistorted images: if the current pixel distance from the image center was smaller than $r = 1024$ (= image radius), the azimuth and elevation angles (φ, θ) of the given pixel were calculated from Eqs. (1) and (2). Then the $\underline{v}$ vector was interpolated from the calibration array of the $\underline{u}_{i,j}$ vectors [Eq. (3)]. Finally, the coordinates of the pixel, which had the correct color on the photograph, were calculated by summarizing the position of the given pixel and the $\underline{v}$ vector of the interpolation. The red, green, and blue values were read out of there and were loaded into the new image at the given pixel position. The two lowest horizontal circles of the CI corresponding to $\theta = 0°$ ($j = 0$) and $5°$ ($j = 1$) were out of the spherical dome and could not be photographed. For pixels with an elevation lower than 10°, extrapolation was used instead of interpolation. (Figure 4D shows the result of such an undistortion on the CI itself.) With this calibration method the result of the undistorted fisheye photograph of any arbitrary image was practically identical to the original (Figs. 4A and 4D) with an accuracy of maximum 2 pixels ($2/2048 \times 180° = 0.18°$).

All situations with the green laser spot positioned by the test person on the planetarium dome were photographed, and these photos were transformed to be undistorted as described above. Then, the red, violet, and blue calibration spots were detected both on the photograph and the original image. The average azimuth differences φ_{cal} between the azimuths of the calibration spots with the same colors on both images were calculated. The whole image was rotated by $-\varphi_{\mathrm{cal}}$ to overlap with the originally generated image, which was projected in the corresponding situation. Thereafter the green laser spot was detected, and its (φ, θ) coordinates were calculated. Then the azimuth error $\Delta\varphi = \varphi - \varphi_{\mathrm{S}}$ and the elevation error $\Delta\theta = \theta - \theta_{\mathrm{S}}$ of sun localization were obtained. For each test person and situation the four free parameters $(\theta_{\mathrm{S}}, \gamma_1, \gamma_2, \delta)$ and the values of $\Delta\varphi$ and $\Delta\theta$ were saved. The distributions of $\Delta\varphi$ and $\Delta\theta$ under various measurement situations were analyzed by circular statistics [22]. The direction and the length R of the average vector of the azimuth and elevation errors $\Delta\varphi$ and $\Delta\theta$ were calculated. Their dispersion was defined as $1 - R$ [22].

C. Accuracy of Estimating the Compass Direction

Using the azimuth and elevation errors $\Delta\varphi$ and $\Delta\theta$ of the estimated sun position $(\varphi_{\mathrm{S}}, \theta_{\mathrm{S}})$, we calculated the error $\Delta\omega_{\mathrm{North}}$ of the estimated northern direction relative to the true north ω_{North}. If there were no sun localization errors ($\Delta\varphi = 0$, $\Delta\theta = 0$), the tip of the gnomon shadow would fall on the appropriate gnomonic line engraved in the disk of the Viking sun-compass, and the mirror symmetry axis of the gnomonic line would point toward the geographic north (Fig. 1C). Because of an inaccurately estimated sun position ($\Delta\varphi \neq 0$, $\Delta\theta \neq 0$), the shadow tip does not fall on the gnomonic line. In this case the sun-compass disk should be rotated by angle $\Delta\omega_{\mathrm{North}}$ around its vertical axis in order that the shadow tip falls on the gnomonic line (Fig. 1C). $\Delta\omega_{\mathrm{North}}$ was calculated for all measurement situations and the 11 test persons for gnomonic lines valid at spring equinox (21 March) and summer solstice (21 June) at the 61° northern latitude. These gnomonic lines were calculated with the program developed by Bernáth *et al.* [4]. The position of the tip of the gnomon shadow on the horizontal sun-compass disk was calculated with a self-developed program. Since a given solar elevation angle θ_{S} can occur twice a day (in the morning and in the afternoon), we calculated two different values of $\Delta\omega_{\mathrm{North}}$ for a given measurement situation. We characterized the $\Delta\omega_{\mathrm{North}}$ values under various measurement situations by circular statistics [22]. We did not calculate $\Delta\omega_{\mathrm{North}}$ for the equinox in measurement situations with high solar elevation angles θ_{S}, which never occur at the 61° latitude in this period.

3. RESULTS

Figure 5 shows the azimuth errors $\Delta\varphi$ (Fig. 5A) and elevation errors $\Delta\theta$ (Fig. 5B) of 2640 measurements performed with the 11 test persons. The solar azimuth angle φ_{S} was estimated with an average error $\Delta\varphi_{\mathrm{average}} = -0.13°$ (Fig. 5A). In some cases the test persons located the antisolar point instead of the sun; therefore there are also some data points around $\Delta\varphi = \pm 180°$ in Figs. 5A and 5C. According to Fig. 5B, the solar elevation angle θ_{S} was estimated with an average error $\Delta\theta_{\mathrm{average}} = +4.47°$ with a clear tendency of overestimation.

Figures 6A and 6B show the averages $\Delta\varphi_{\mathrm{average}}$ and $\Delta\theta_{\mathrm{average}}$ of the azimuth errors $\Delta\varphi$ and elevation errors $\Delta\theta$ of the 11 test persons studied. The directions and lengths R of the average vectors $\Delta\varphi_{\mathrm{average}}$ and $\Delta\theta_{\mathrm{average}}$ are summarized in Table 2. The most accurate solar azimuth estimation was performed by test person 10 with $\Delta\varphi_{\mathrm{average}} = -0.14°$, but he detected the sun with a relatively high dispersion $1 - R_{\mathrm{azimuth}} = 0.392$. The least

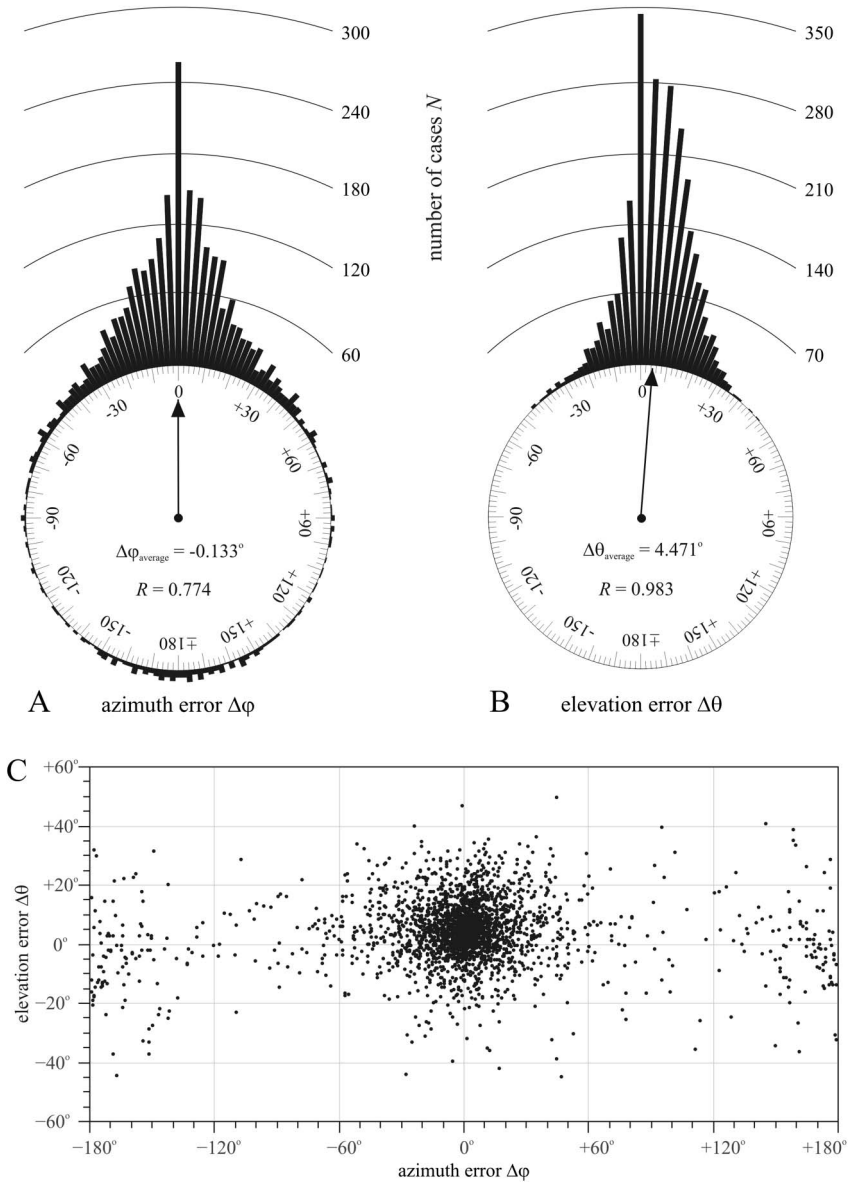

Fig. 5. A, B, circular histograms (radial, number of cases N; azimuthal, angle, bin width = 2°) of the azimuth errors $\Delta\varphi$ and elevation errors $\Delta\theta$ of sun localization by 11 test persons in our planetarium experiment. Black arrows show the directions of the average error vectors, the length of which is R. C, plot of $\Delta\theta$ versus $\Delta\varphi$ showing the scatter of both errors.

accurate solar azimuth estimation was performed by test person 6 with $\Delta\varphi_{\text{average}} = -3.86°$, and test person 11 with $\Delta\theta_{\text{average}} = 8.81°$ was the least accurate in the estimation of solar elevation. The smallest and largest azimuth dispersion $1 - R_{\text{azimuth}}$ was 0.119 and 0.427, respectively. According to Fig. 6B and Table 2, the most accurate solar elevation estimation was performed with an error of $\Delta\theta_{\text{average}} = 0.58°$. The smallest and largest elevation dispersion $1 - R_{\text{elevation}}$ was 0.010 and 0.028, respectively.

The direction and length R of the compass direction error $\Delta\omega_{\text{North}}$ of the 11 test persons for the spring equinox (21 March) and summer solstice (21 June) are also summarized in Table 2. We found that the values of $\Delta\omega_{\text{North}}$ were smaller at solstice than at equinox. In other words, the test persons could determine the northern direction more accurately at solstice. In the estimation of the northern direction the smallest error was $\Delta\omega_{\text{North}} = 0.06°$ (with $1 - R = 0.283$) at solstice, and $\Delta\omega_{\text{North}} = 0.05°$ (with $1 - R = 0.671$) at equinox. Not surprisingly, the smallest dispersion was found at both solstice ($1 - R = 0.282$) and equinox ($1 - R = 0.569$) for that test person (No. 5) who also estimated the solar azimuth and elevation with the lowest dispersion.

Figure 7 shows the average vectors of the compass direction error $\Delta\omega_{\text{North}}$ in all measurement situations for spring equinox and summer solstice calculated from the azimuth and elevation errors $\Delta\varphi$ and $\Delta\theta$ of the 11 test persons. The direction and length R of the average compass direction errors are summarized in Table 3. At solstice, the most accurate north determination was performed for the following parameter configurations: $35° \le \theta_S \le 55°$, $95° \le \delta \le 115°$, $35° \le \gamma_1 \le 55°$, and $35° \le \gamma_2 \le 55°$ with $\Delta\omega_{\text{North}} = 0.2°$. At equinox, the most exact north determination was achieved for $5° \le \theta_S \le 25°$, $65° \le \delta \le 85°$, $35° \le \gamma_1 \le 55°$, and $35° \le \gamma_2 \le 55°$ with $\Delta\omega_{\text{North}} = 0.1°$. The measurement situation $35° \le \theta_S \le 55°$, $95° \le \delta \le 115°$, $35° \le \gamma_1 \le 55°$, and $65° \le \gamma_2 \le 85°$ was characterized by the smallest dispersion $1 - R = 0.16$

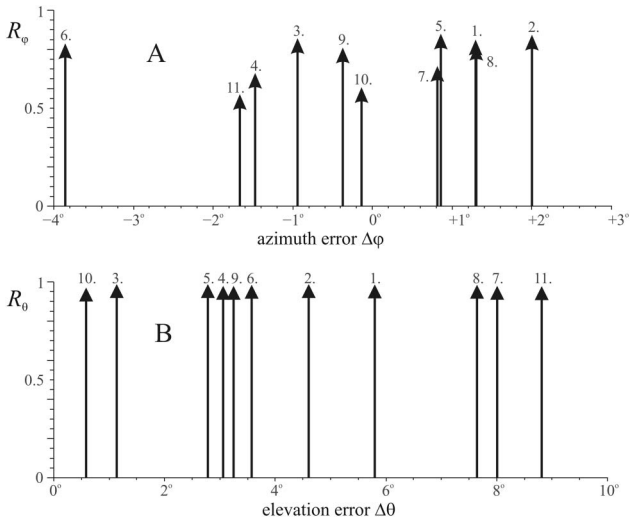

Fig. 6. A, Average vectors of the azimuth error $\Delta\varphi$ and B, elevation error $\Delta\theta$ of the 11 test persons studied in our experiment. The identity numbers of the test persons are at the corresponding arrow heads. R, vector length.

at solstice. Generally, the dispersion values were the largest when the sun elevation was $5° \leq \theta_S \leq 25°$ at equinox. The length R of the average compass error vector was the highest ($R = 0.16$) at equinox in the measurement situation $5° \leq \theta_S \leq 25°$, $125° \leq \delta \leq 145°$, $65° \leq \gamma_1 \leq 85°$, and $95° \leq \gamma_2 \leq 115°$. The following are clearly visible in Fig. 7: (i) north determination was more accurate at solstice, (ii) north estimation was less accurate when γ_1, γ_2, and δ increased, and (iii) north determination was more precise when the solar elevation angle was $35^o \leq \theta_S \leq 55°$.

4. DISCUSSION

The feasibility of the sky-polarimetric Viking navigation strongly depends on the weather conditions [10,16,17]. The climate of the Viking era and area (Scandinavia and the Northern Atlantic) was very different from the present climate in that region [23]. When fog and/or thick clouds occluded the sun and the whole sky was overcast, there was no atmospheric optical phenomenon (e.g., crepuscular rays or cloud shadows) that could help to determine the position of the invisible sun with the naked eye. Landmarks were not available either in the homogenous marine optical environment. According to the hypothesis of sky-polarimetric Viking navigation, in such situations the navigator could align the sunstones in such a way that the skylight seen through a dichroic cordierite or tourmaline crystal should be the brightest (or darkest), or the two images of a sky patch seen through a birefringent calcite crystal should have the same brightness (or the largest brightness difference) [8,10,18]. This crystal alignment is determined by the local direction of skylight polarization in the observed sky patch. According to the theory of first-order Rayleigh scattering, the local direction of skylight polarization is always perpendicular to the great circle crossing the given celestial point and the sun [9,14,19,21]. Under a clear sky with a visible sun, the direction of this great circle can be marked on the sunstone crystal with a straight scratch and used further on as a direction finder (to find the direction towards the invisible sun). The above-horizon intersection of two such celestial great circles always gives the position of the sun. This fact is the basis of the second step of sky-polarimetric Viking navigation. However, under foggy and overcast skies the degree of linear polarization of skylight is so low [16,24] that skylight polarization could not be analyzed with sunstones precisely enough for navigation purposes [10].

When the sky was only partially cloudy and a thick cloud occluded the sun, a Viking navigator could use the sunstones, but frequently was forced to measure the sky polarization in a clear sky patch far enough from the sun (γ_1, $\gamma_2 > 90°$). Our results showed that such a geometrical arrangement decreases the accuracy of sky-polarimetric Viking navigation even if sunstones could be aligned without any error. In such cases the second step of sun localization (estimating the intersection of the two celestial great circles across and parallel to the two scratches on the two sunstones) is inaccurate as we obtained in our planetarium experiment (Figs. 5–7, Tables 2 and 3). In the worst case the navigator could also locate the antisolar point instead of the sun (Fig. 5), as also happened in the field tests performed by Bernáth *et al.* [10]. This mistake

Table 2. Average Azimuth Error $\Delta\varphi_{\text{average}}$, Average Elevation Error $\Delta\theta_{\text{average}}$, Average Compass Direction Error $\Delta\omega_{\text{North}}$, and the Length R of These Error Vectors Measured for the 11 Test Persons in Our Experiment for Spring Equinox (21 March) and Summer Solstice (21 June)[a]

	Azimuth Error		Elevation Error		Compass Direction Error at Spring Equinox (21 March)			Compass Direction Error at Summer Solstice (21 June)		
Test Person	$\Delta\varphi_{\text{average}}$	R_{azimuth}	$\Delta\theta_{\text{average}}$	$R_{\text{elevation}}$	$\Delta\omega_{\text{North}}$	R	n	$\Delta\omega_{\text{North}}$	R	n
1.	1.29°	0.852	5.79°	0.987	0.29°	0.401	240	1.64°	0.628	450
2.	1.99°	0.875	4.60°	0.989	2.81°	0.427	240	3.09°	0.639	450
3.	−0.95°	0.858	1.13°	0.989	0.91°	0.411	240	0.06°	0.717	450
4.	−1.48°	0.681	3.06°	0.980	0.05°	0.329	240	−0.32°	0.630	450
5.	0.86°	0.881	2.77°	0.990	2.77°	0.431	240	0.50°	0.718	450
6.	−3.86°	0.832	3.56°	0.987	−2.52°	0.419	240	−3.34°	0.650	450
7.	0.81°	0.716	8.00°	0.980	−1.36°	0.335	240	0.83°	0.549	450
8.	1.30°	0.825	7.64°	0.986	1.06°	0.411	240	0.25°	0.616	450
9.	−0.38°	0.810	3.24°	0.981	1.09°	0.351	240	−1.28°	0.683	450
10.	−0.14°	0.608	0.58°	0.972	3.25°	0.166	240	−0.86°	0.691	450
11.	−1.67°	0.573	8.81°	0.979	6.29°	0.193	240	−1.33°	0.564	450

[a] n is the number of situations in which we calculated $\Delta\omega_{\text{North}}$.

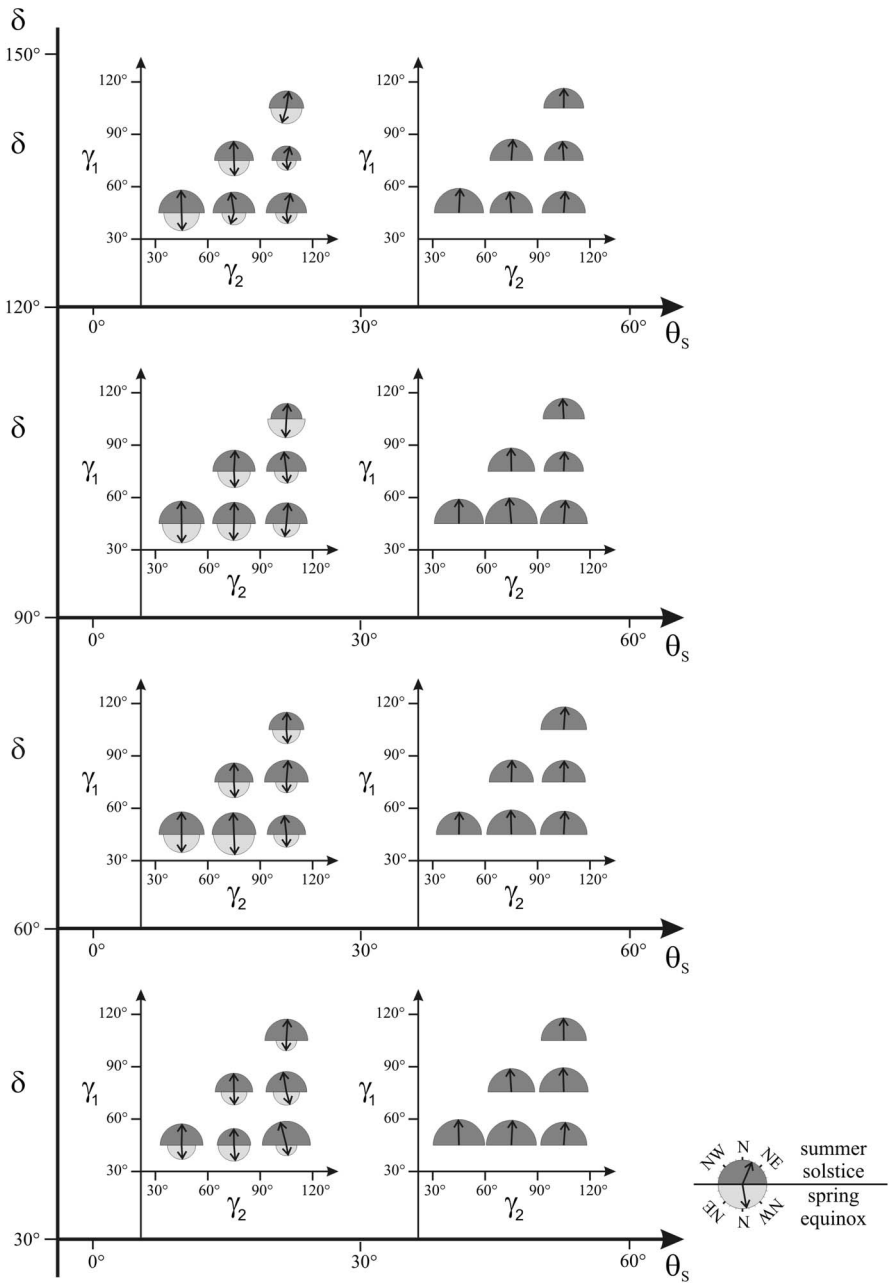

Fig. 7. Average vectors of the compass direction error $\Delta\omega_{\mathrm{North}}$ in all measurement situations at spring equinox (21 March) and summer solstice (21 June) at the 61° latitude calculated from the azimuth and elevation errors $\Delta\varphi$ and $\Delta\theta$ of the 11 test persons studied. Black arrows show the directions of the average error vectors $\Delta\omega_{\mathrm{North}}$. The radius of the semicircles is proportional to the length R of the average vectors. The average vectors of $\Delta\omega_{\mathrm{North}}$ belonging to spring equinox are rotated by 180° for the sake of a better visualization.

is more frequent when the sun is closer to the horizon. In the field the brighter sky region around the sun can prevent such mistakes.

In our experiment the solar elevation angle θ_S was estimated with a clear tendency of slight overestimation, meaning predominantly positive $\Delta\theta$ values (Fig. 5B). It is improbable that the bottom of the planetarium dome seen slightly above the eye level of the test persons confused them, because such an overestimation of the elevation of the invisible sun has also been observed in two earlier outdoor psychophysical experiments [5,10] studying different aspects of sky-polarimetric Viking navigation. Although the human brain is accustomed to challenges that are solvable with Euclidean geometry, the estimation of the intersection of two celestial great circles is a rather strange, unusual task: on the one hand, human observers (test persons) may tend to elongate the two black bars (representing the scratches on the two sunstones) projected on the planetarium dome (representing the sky) into two straight lines instead of celestial great circles. On the other hand, humans usually overestimate vertical distances, one of the consequences of which is the well-known moon illusion [25,26]. Both phenomena lead to a wrong estimation of the sun position.

We found that the most precise north determination happened at the highest solar elevation, and the accuracy of this task decreased if angles γ_1 and γ_2 of the projected black bars

Table 3. Average Compass Direction Errors $\Delta\omega_{\mathrm{North}}$ and the Length R of these Error Vectors Measured in All Measurement Situations for Spring Equinox (21 March) and Summer Solstice (21 June)[a]

Measurement Situations				Compass Direction Error at Spring Equinox (21 March)			Compass Direction Error at Summer Solstice (21 June)		
θ_S	γ_1	γ_2	δ	$\Delta\omega_{\mathrm{North}}$	R	n	$\Delta\omega_{\mathrm{North}}$	R	n
5°–25°	35°–55°	35°–55°	35°–55°	3.4°	0.34	110	−1.2°	0.64	110
5°–25°	65°–85°	65°–85°	35°–55°	1.9°	0.29	110	1.0°	0.53	110
5°–25°	95°–115°	95°–115°	35°–55°	−1.5°	0.18	110	−3.2°	0.64	110
5°–25°	35°–55°	65°–85°	35°–55°	4.9°	0.41	110	0.8°	0.46	110
5°–25°	35°–55°	95°–115°	35°–55°	10.2°	0.19	110	14.6°	0.76	110
5°–25°	65°–85°	95°–115°	35°–55°	15.6°	0.31	110	9.4°	0.60	110
5°–25°	35°–55°	35°–55°	65°–85°	0.1°	0.50	110	0.3°	0.69	110
5°–25°	65°–85°	65°–85°	65°–85°	3.9°	0.41	110	−0.5°	0.55	110
5°–25°	95°–115°	95°–115°	65°–85°	5.3°	0.33	110	−1.8°	0.48	110
5°–25°	35°–55°	65°–85°	65°–85°	2.4°	0.60	110	2.2°	0.66	110
5°–25°	35°–55°	95°–115°	65°–85°	1.1°	0.29	110	6.5°	0.56	110
5°–25°	65°–85°	95°–115°	65°–85°	3.5°	0.20	110	−4.4°	0.67	110
5°–25°	35°–55°	35°–55°	95°–115°	0.5°	0.55	110	0.7°	0.69	110
5°–25°	65°–85°	65°–85°	95°–115°	3.1°	0.44	110	−3.0°	0.63	110
5°–25°	95°–115°	95°–115°	95°–115°	−2.9°	0.54	110	−4.9°	0.40	110
5°–25°	35°–55°	65°–85°	95°–115°	−1.8°	0.45	110	−0.7°	0.64	110
5°–25°	35°–55°	95°–115°	95°–115°	−7.0°	0.31	110	−4.8°	0.62	110
5°–25°	65°–85°	95°–115°	95°–115°	5.5°	0.25	110	7.1°	0.59	110
5°–25°	35°–55°	35°–55°	125°–145°	2.0°	0.49	110	1.3°	0.70	110
5°–25°	65°–85°	65°–85°	125°–145°	2.4°	0.39	110	1.1°	0.56	110
5°–25°	95°–115°	95°–115°	125°–145°	−16.3°	0.40	110	−8.0°	0.48	110
5°–25°	35°–55°	65°–85°	125°–145°	−16.5°	0.26	110	8.5°	0.62	110
5°–25°	35°–55°	95°–115°	125°–145°	7.6°	0.20	110	−11.4°	0.60	110
5°–25°	65°–85°	95°–115°	125°–145°	8.1°	0.16	110	−12.9°	0.56	110
35°–55°	35°–55°	35°–55°	35°–55°	—	—	0	1.4°	0.82	88
35°–55°	65°–85°	65°–85°	35°–55°	—	—	0	3.7°	0.72	88
35°–55°	95°–115°	95°–115°	35°–55°	—	—	0	0.6°	0.69	110
35°–55°	35°–55°	65°–85°	35°–55°	—	—	0	−2.8°	0.80	110
35°–55°	35°–55°	95°–115°	35°–55°	—	—	0	−4.0°	0.72	110
35°–55°	65°–85°	95°–115°	35°–55°	—	—	0	1.5°	0.76	88
35°–55°	35°–55°	35°–55°	65°–85°	—	—	0	−0.8°	0.69	110
35°–55°	65°–85°	65°–85°	65°–85°	—	—	0	−1.5°	0.67	66
35°–55°	95°–115°	95°–115°	65°–85°	—	—	0	−3.8°	0.71	110
35°–55°	35°–55°	65°–85°	65°–85°	—	—	0	1.4°	0.78	88
35°–55°	35°–55°	95°–115°	65°–85°	—	—	0	−2.9°	0.72	110
35°–55°	65°–85°	95°–115°	65°–85°	—	—	0	−1.1°	0.65	110
35°–55°	35°–55°	35°–55°	95°–115°	—	—	0	0.2°	0.78	88
35°–55°	65°–85°	65°–85°	95°–115°	—	—	0	0.9°	0.72	110
35°–55°	95°–115°	95°–115°	95°–115°	—	—	0	3.0°	0.61	88
35°–55°	35°–55°	65°–85°	95°–115°	—	—	0	4.8°	0.84	110
35°–55°	35°–55°	95°–115°	95°–115°	—	—	0	−4.2°	0.73	66
35°–55°	65°–85°	95°–115°	95°–115°	—	—	0	−2.3°	0.58	88
35°–55°	35°–55°	35°–55°	125°–145°	—	—	0	−2.6°	0.78	66
35°–55°	65°–85°	65°–85°	125°–145°	—	—	0	−4.4°	0.64	88
35°–55°	95°–115°	95°–115°	125°–145°	—	—	0	−0.4°	0.59	110
35°–55°	35°–55°	65°–85°	125°–145°	—	—	0	4.9°	0.64	88
35°–55°	35°–55°	95°–115°	125°–145°	—	—	0	−3.9°	0.65	110
35°–55°	65°–85°	95°–115°	125°–145°	—	—	0	3.9°	0.57	110

[a] n is the number of situations when $\Delta\omega_{\mathrm{North}}$ was determined.

(sunstones) from the sun and angle δ between the planes of the two celestial great circles increased. These findings can be explained by the limited field of view of the human eye: if the navigator cannot choose two nearby sky points for the sunstone analysis because of foggy or cloudy meteorological conditions, he has to determine the direction of skylight polarization at distant celestial points. In this case he has to rotate his head a lot, which leads to inaccuracies in the estimation of angles and directions on the sky dome. The navigator can determine the above-horizon intersection of the two celestial great circles more easily if the two selected sky points are closer to each other and the sun, and these three celestial points have higher elevations.

The compass direction error $\Delta\omega_{\mathrm{North}}$ caused by the inaccurate estimation of the sun position depends on the method of deriving the geographical north. If this method is based on fitting the gnomon's shadow tip to a gnomonic line on the Viking sun-compass (Fig. 1C), $\Delta\omega_{\mathrm{North}}$ is greatly influenced by the

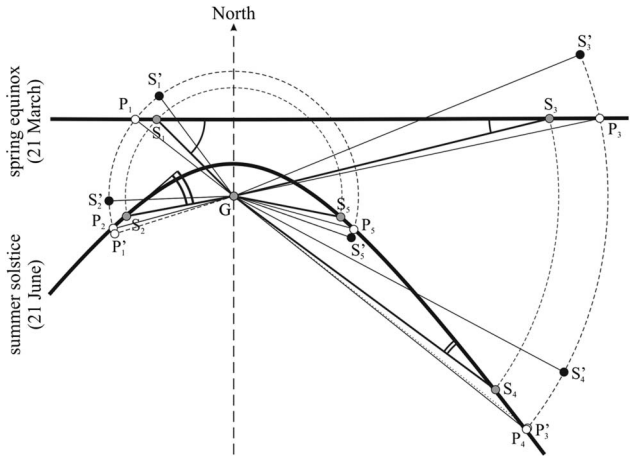

Fig. 8. On a precisely orientated Viking sun-compass the gnomon's shadow tip S_n ($n = 1, 2, 3, 4, 5$) falls on the gnomonic line (thick solid lines), the mirror symmetry axis of which (dashed line) marks the true north. The estimated shadow tip S'_n ($n = 1, 2, 3, 4, 5$) is off the gnomonic line; thus the compass should be rotated along its vertical axis by an angle $\Delta\omega_{\mathrm{North}} \equiv P_n G S'_n$ (called the compass direction error) between radii GP_n and GS'_n in order to move S'_n to the gnomonic point P_n. If all the angles $S_n G S'_n$ are identical, angle $P_n G S'_n$ is proportional to the angles enclosed by the shadow GS_n and the gnomonic line marked by single arcs for the spring equinox (A, 21 March) and by double arcs for the summer solstice (B, 21 June). At solstice, rotating the sun-compass by $\Delta\omega_{\mathrm{North}}$ valid for equinox ($P_1 G S'_1$ or $P_3 G S'_3$) moves the estimated shadow tip (S'_2 and S'_4) off the gnomonic line (P'_1 and P'_3). Identical solar elevation angle, azimuth error, and elevation error results in different $\Delta\omega_{\mathrm{North}}$ in the morning ($P_2 G S'_2$) and in the afternoon ($P_5 G S'_5$).

geometrical arrangement of the shadow and the gnomonic line (Fig. 8). Identical sun position errors result in different distances between the estimated shadow tip and the gnomonic line. At higher solar elevations the linear equinox line (valid on 21 March) is farther from the shadow tip than the hyperbolic solstice line (valid on 21 June); thus smaller $\Delta\omega_{\mathrm{North}}$ values occur in summer than in spring. The relationship is the opposite at lower solar elevations.

Our test persons estimated the solar elevation more precisely (with smaller $\Delta\theta$) than the solar azimuth (with larger $\Delta\varphi$). However, even small solar elevation errors $\Delta\theta$ can cause great compass direction errors $\Delta\omega_{\mathrm{North}}$. This is most explicit when the sun is close to the horizon, because then even small changes in the solar elevation θ_{S} can result in great changes in the shadow length; thus the estimated shadow tip falls far off the actual gnomonic line. Since in such situations our test persons estimated the sun position with great errors, the compass direction errors $\Delta\omega_{\mathrm{North}}$ can be extremely large.

Although the planetarium dome was homogeneous white, a pale radial pattern was visible on it (Figs. 3A–3C), because the dome canvas was composed of several sectors. Unfortunately, we could not eliminate this faint grid, which thus was seen by the test persons when confronted with the task to mentally project great circles through the black bars. The appearance of such a dim white grid pattern could slightly (mis)lead test subjects in their task.

In the second step of sky-polarimetric Viking navigation the task is to cross great circles directed by the local direction of skylight polarization. This procedure would be more accurate if such matching were done through more than two celestial points, that is, observing polarization at various points in the sky. However, doing so in a simultaneous fashion would be very problematic in reality (aboard a ship on the open sea) without some device with a rigid construction where the sunstones are not handheld by the navigator rather than mounted to some poles, for example, where they can be freely rotated. Without such an additional device (lacking any archeological evidence), the navigator could simultaneously measure sky polarization only with two sunstones held in his two hands.

Our test persons were ordinary people who never had to execute an orientation task before that even closely resembled the procedure required for sky-polarimetric Viking navigation. In the future it would be beneficial to study how test subjects would perform after thorough training. It is obvious that an experienced Viking navigator had smaller errors than our test persons. Thus, in our investigation the accuracy of the second step of sky-polarimetric Viking navigation was underestimated relative to that of trained polarimetric navigators.

In another psychophysical laboratory experiment we studied the accuracy of the first step of sky-polarimetric Viking navigation (Fig. 1A), i.e., how accurately test persons can adjust the appropriate alignment of birefringent calcite and dichroic cordierite and tourmaline crystals as a function of the degree of linear polarization of incident white light if they try to find the crystal alignment when the skylight seen through a cordierite or tourmaline sunstone is the brightest (or darkest), or the two images of a sky patch seen through a calcite sunstone have the same brightness (or the largest brightness difference). The results of this investigation will be published in a separate paper. Due to the different origin and quality of these sunstone crystals, and to the sensitivity of the human eye, the first step of sky-polarimetric Viking navigation is also crucial, like the third step (Fig. 1C). Our final goal is to determine the net error of sky-polarimetric Viking navigation, namely, how precisely experienced navigators can determine the geographic northern direction with two sunstones and a sun-compass at a given latitude and under different sky conditions. The results presented in this work contribute to this challenging aim.

5. CONCLUSION

We conclude that in the second step of the hypothetic sky-polarimetric Viking navigation the sun position (solar elevation θ_{S}, solar azimuth φ_{S}) can be estimated by means of a pair of sunstones with straight scratches pointing toward the invisible sun with an average error of $+0.58° \le \Delta\theta \le +8.81°$ and $-3.86° \le \Delta\varphi \le +1.99°$. The northern direction (ω_{North}) was determined by the 11 test persons with an error of $-3.34° \le \Delta\omega_{\mathrm{North}} \le +6.29°$. The inaccuracy of this navigation method was high ($\Delta\omega_{\mathrm{North}} = -16.3°$) when the solar elevation was $5° \le \theta_{\mathrm{S}} \le 25°$, and the two selected celestial points were far from the sun (at angular distances $95° \le \gamma_1, \gamma_2 \le 115°$) and each other ($125° \le \delta \le 145°$). Hence, considering only the second step, the alleged sky-polarimetric Viking navigation could be more practical/accurate in the mid-summer period (June and July), when in the daytime the sun is high above the horizon for long periods. In the spring (and autumn) equinoctial period, alternative methods (using a twilight board, for example, [5]) might be more appropriate. Since Viking navigators surely also committed further errors in the first and third steps, the orientation errors presented here underestimate the net error of the whole sky-polarimetric navigation.

ACKNOWLEDGMENTS

This work was supported by grant OTKA K-105054 (Full-Sky Imaging Polarimetry to Detect Clouds and to Study the Meteorological Conditions Favourable for Polarimetric Viking Navigation) received by G. Horváth from the Hungarian Science Foundation. Gábor Horváth also thanks the German Alexander von Humboldt Foundation for an equipment donation. Balázs Bernáth is grateful for the research fellowship 3.3-UNG/1127933STP received from the Alexander von Humboldt Foundation, and for the project support 12.153 from the Swiss CRUS Scientific Exchange Programme NMS-CH. We are grateful to Prof. Kristóf Petrovay, head of the Department of Astronomy of the Eötvös University (Budapest), who made the planetarium of Eötvös University available to our experiment. We thank the 11 test persons for their cooperation. We are grateful to an anonymous reviewer for her/his constructive and valuable comments.

REFERENCES

1. T. H. McGovern, "The archeology of the Norse North Atlantic," Annu. Rev. Anthropol. **19**, 331–351 (1990).
2. O. Olsen and O. Crumlin-Pedersen, *Five Viking Ships from Roskilde Fjord* (National Museum, 1978).
3. S. Thirslund, *Viking Navigation: Sun-Compass Guided Norsemen First to America* (Gullanders Bogtrykkeri a-s, 2001).
4. B. Bernáth, M. Blahó, Á. Egri, A. Barta, and G. Horváth, "An alternative interpretation of the Viking sundial artefact: an instrument to determine latitude and local noon," Proc. R. Soc. A **469**, 20130021 (2013).
5. B. Bernáth, A. Farkas, D. Száz, M. Blahó, Á. Egri, A. Barta, S. Åkesson, and G. Horváth, "How could the Viking sun-compass be used with sunstones before and after sunset? Twilight board as a new interpretation of the Uunartoq artefact fragment," Proc. R. Soc. A **470**, 20130787 (2014).
6. T. Ramskou, "Solstenen," Skalk **2**, 16–17 (1967).
7. P. G. Foote, "Icelandic sólarsteinn and the Medieval background," J. Scandinavian Folklore **12**, 26–40 (1956).
8. A. Le Floch, G. Ropars, J. Lucas, S. Wright, T. Davenport, M. Corfield, and M. Harrisson, "The sixteenth century Alderney crystal: a calcite as an efficient reference optical compass?" Proc. R. Soc. A **469**, 20120651 (2013).
9. K. L. Coulson, *Polarization and Intensity of Light in the Atmosphere* (A. Deepak, 1988).
10. B. Bernáth, M. Blahó, Á. Egri, A. Barta, G. Kriska, and G. Horváth, "Orientation with a Viking sun-compass, a shadow-stick and calcite sunstones under various weather situations," Appl. Opt. **52**, 6185–6194 (2013).
11. C. Roslund and C. Beckman, "Disputing Viking navigation by polarized skylight," Appl. Opt. **33**, 4754–4755 (1994).
12. I. Pomozi, G. Horváth, and R. Wehner, "How the clear-sky angle of polarization pattern continues underneath clouds: full-sky measurements and implications for animal orientation," J. Exp. Biol. **204**, 2933–2942 (2001).
13. L. K. Karlsen, *Secrets of the Viking Navigators* (One Earth, 2003).
14. B. Suhai and G. Horváth, "How well does the Rayleigh model describe the E-vector distribution of skylight in clear and cloudy conditions? A full-sky polarimetric study," J. Opt. Soc. Am. A **21**, 1669–1676 (2004).
15. A. Barta, G. Horváth, and V. B. Meyer-Rochow, "Psychophysical study of the visual sun location in pictures of cloudy and twilight skies inspired by Viking navigation," J. Opt. Soc. Am. A **22**, 1023–1034 (2005).
16. R. Hegedüs, S. Åkesson, R. Wehner, and G. Horváth, "Could Vikings have navigated under foggy and cloudy conditions by skylight polarization? On the atmospheric optical prerequisites of polarimetric Viking navigation under foggy and cloudy skies," Proc. R. Soc. A **463**, 1081–1095 (2007).
17. G. Horváth, A. Barta, I. Pomozi, B. Suhai, R. Hegedüs, S. Åkesson, V. B. Meyer-Rochow, and R. Wehner, "On the trail of Vikings with polarized skylight: experimental study of the atmospheric optical prerequisites allowing polarimetric navigation by Viking seafarers," Phil. Trans. R. Soc. B **366**, 772–782 (2011).
18. G. Ropars, G. Gorre, A. Le Floch, J. Enoch, and V. Lakshminarayanan, "A depolarizer as a possible precise sunstone for Viking navigation by polarized skylight," Proc. R. Soc. A **468**, 671–684 (2012).
19. G. P. Können, *Polarized Light in Nature* (Cambridge University, 1985).
20. G. Horváth, B. Bernáth, B. Suhai, A. Barta, and R. Wehner, "First observation of the fourth neutral polarization point in the atmosphere," J. Opt. Soc. Am. A **19**, 2085–2099 (2002).
21. G. Horváth and D. Varjú, *Polarized Light in Animal Vision—Polarization Patterns in Nature* (Springer Verlag, 2004).
22. E. Batschelet, *Circular Statistics in Biology* (Academic, 1981).
23. A. E. J. Ogilvie, L. K. Barlow, and A. E. Jennings, "North Atlantic climate c. ad. 1000: millennial reflections on the Viking discoveries of Iceland, Greenland and North America," Weather **55**, 34–45 (2000).
24. R. Hegedüs, S. Åkesson, and G. Horváth, "Polarization patterns of thick clouds: overcast skies have distribution of the angle of polarization similar to that of clear skies," J. Opt. Soc. Am. A **24**, 2347–2356 (2007).
25. R. Kammann, "The overestimation of vertical distance and slope and its role in the moon illusion," Perception Psychophys. **2**, 585–589 (1967).
26. M. Hershenson, *The Moon Illusion* (Erlbaum, 1989).